AGU PUBLICATIONS

JGR

Journal of Geophysical Research: Planets

RESEARCH ARTICLE

10.1002/2016JE005254

Key Points:
- Crater statistics constrain the onset of Mercury's two most recent periods
- Results indicate younger Kuiperian and Mansurian periods than previously assumed
- The Kuiperian likely began ~280 ± 60 Ma and the Mansurian ~1.7 ± 0.2 Ga

Supporting Information:
- Supporting Information S1
- Figure S1
- Figure S2
- Figure S3
- Figure S4
- Table S1
- Table S2

Correspondence to:
M. E. Banks,
maria.e.banks@nasa.gov

Citation:
Banks, M. E., Z. Xiao, S. E. Braden, N. G. Barlow, C. R. Chapman, C. I. Fassett, and S. S. Marchi (2017), Revised constraints on absolute age limits for Mercury's Kuiperian and Mansurian stratigraphic systems, *J. Geophys. Res. Planets*, *122*, 1010–1020, doi:10.1002/2016JE005254.

Received 31 DEC 2016
Accepted 13 APR 2017
Accepted article online 18 APR 2017
Published online 26 MAY 2017

Revised constraints on absolute age limits for Mercury's Kuiperian and Mansurian stratigraphic systems

Maria E. Banks[1,2,3], Zhiyong Xiao[4,5], Sarah E. Braden[6], Nadine G. Barlow[7], Clark R. Chapman[8], Caleb I. Fassett[9], and Simone S. Marchi[10]

[1]NASA Goddard Space Flight Center, Greenbelt, Maryland, USA, [2]Center for Earth and Planetary Studies, National Air and Space Museum, Smithsonian Institution, Washington, District of Columbia, USA, [3]Planetary Science Institute, Tucson, Arizona, USA, [4]School of Earth Sciences, China University of Geosciences, Wuhan, China, [5]Centre for Earth Evolution and Dynamics, University of Oslo, Oslo, Norway, [6]School of Earth and Space Exploration, Arizona State University, Tempe, Arizona, USA, [7]Department of Physics and Astronomy, Northern Arizona University, Flagstaff, Arizona, USA, [8]Department of Space Studies, Southwest Research Institute, Boulder, Colorado, USA, [9]NASA Marshall Space Flight Center, Huntsville, Alabama, USA, [10]NASA Lunar Science Institute, Southwest Research Institute, Boulder, Colorado, USA

Abstract Following an approach similar to that used for the Moon, Mercury's surface units were subdivided into five time-stratigraphic systems based on geologic mapping using Mariner 10 images. The absolute time scale originally suggested for the time periods associated with these systems was based on the assumption that the lunar impact flux history applied to Mercury. However, we find that the duration and onset of corresponding periods in the stratigraphic sequences on Mercury and the Moon are not the same. Using high-resolution and multiband image data obtained by the MErcury Surface, Space ENviroment, GEochemistry, and Ranging (MESSENGER) spacecraft, we identify and catalog fresh impact craters interpreted to have formed during Mercury's two most recent periods, the Mansurian and Kuiperian. We use the densities of the inferred Kuiperian- and Mansurian-aged crater populations to estimate new limits for the age boundaries of these time intervals. Results suggest that both the Mansurian and Kuiperian periods began more recently and extended for significantly shorter durations of time than previously suggested. The Kuiperian is estimated to have initiated as recently as ~280 ± 60 Ma and the Mansurian as recently as ~1.7 ± 0.2 Ga.

1. Introduction

Based on morphologically distinct basin and crater deposits observed in Mariner 10 data, *Spudis and Guest* [1988] subdivided Mercury's surface units into five time-stratigraphic systems using an approach similar to that of *Shoemaker and Hackman* [1962] in defining a chronostratigraphic classification for the Moon. *Spudis and Guest* [1988] suggested initial approximate age limits for the time periods associated with Mercury's stratigraphic systems based on analogy with the Moon and the assumption of a lunar impact flux history [*Wilhelms*, 1987]. From oldest to youngest, these are the pre-Tolstojan (>~4.0 Ga), Tolstojan (~4.0 to ~3.9 Ga), Calorian (~3.9 to ~3.5–3.0 Ga), Mansurian (~3.5–3.0 to ~1.0 Ga), and Kuiperian (<~1.0 Ga).

Mercury's pre-Tolstojan system includes ancient multiring basins and extensive intercrater plains materials, while the Tolstojan, the base of which is defined by the Tolstoj basin (~356 km in diameter), includes Mercury's oldest smooth plains materials [*Spudis and Guest*, 1988]. The Caloris basin (~1525 km in diameter), thought to date from near the end of the late heavy bombardment (LHB) of the inner solar system [e.g., *Strom et al.*, 2005], defines the base of the Calorian system and includes Mercury's youngest widespread smooth volcanic plains deposits [*Spudis and Guest*, 1988]. The Mansurian and Kuiperian systems are defined as including impact crater-related landforms and deposits typified by the craters Mansur (~75 km in diameter) and Kuiper (~62 km in diameter), respectively. The Mansurian includes only minor plains materials confined to crater floors and relatively fresh craters that appear only slightly degraded (Figure 1) [*Spudis and Guest*, 1988; *Denevi and Robinson*, 2008; *Braden and Robinson*, 2013]. *Spudis and Guest* [1988] include this description of the population of craters that formed during this period: "Mansurian-age craters possess no rays, but fine-scale structures in their ejecta deposits are largely preserved. All craters of this age are randomly distributed over the planet and no regional plains of Mansurian age have been recognized." *Spudis and Guest* [1988] suggest that the formation of Mansur crater marks the base of the Mansurian, but, as this is not a global marker, we focus here on their definition of the Mansurian as the time period during which the global population of

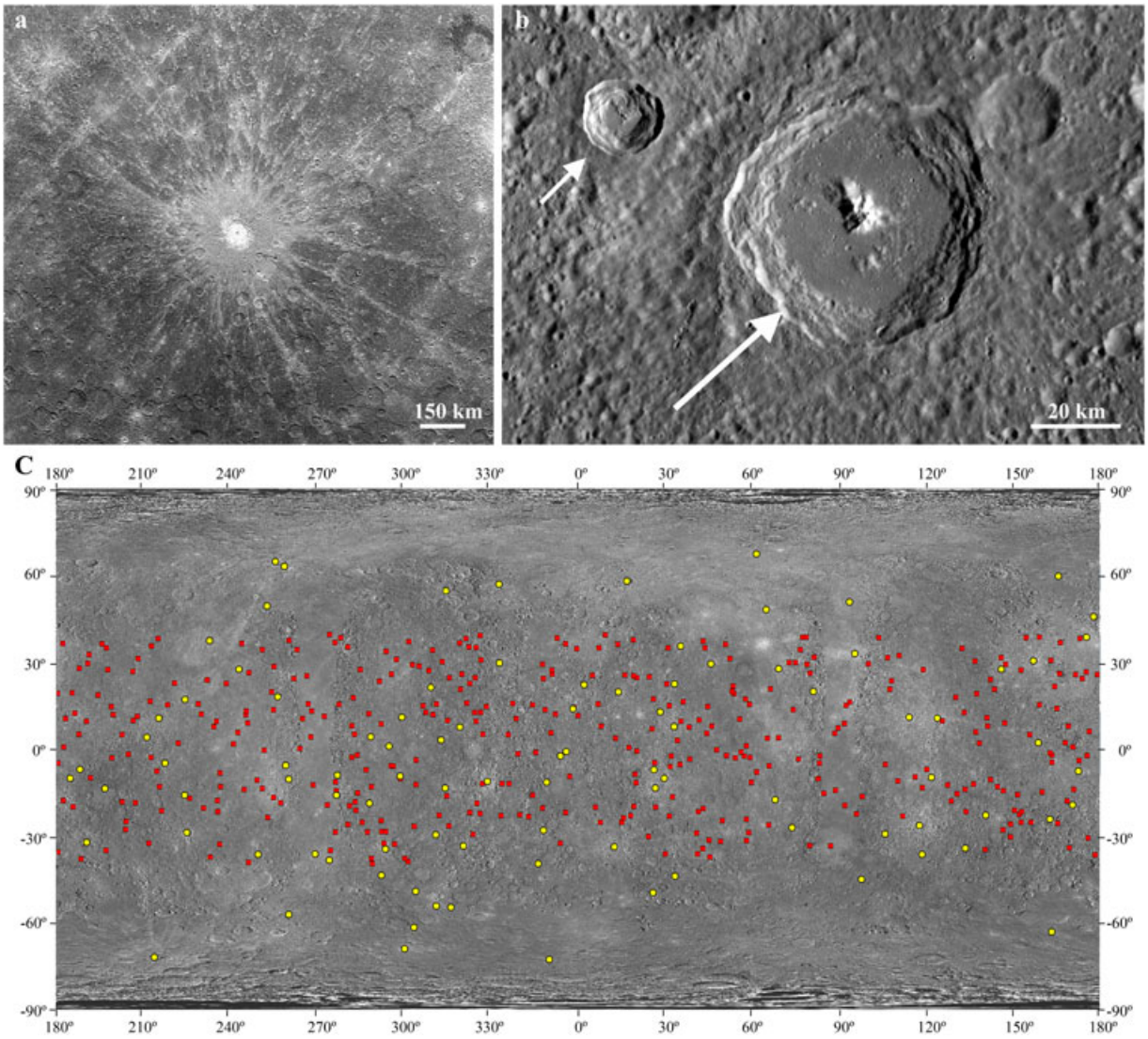

Figure 1. Fresh craters on Mercury. (a) Debussy, a Kuiperian rayed crater (~80 km in diameter; 34.0°S, 12.5°E; MDIS image EW0209886978I). (b) Close-up of a Mansurian crater (~55 km in diameter; larger and long arrow; 9.8°N, 41.8°E; MDIS image mosaic), and a Kuiperian crater (~18 km in diameter; optical rays not visible in this view; small and short arrow; 10.4°N, 40.6°E). (c) Fresh craters used in this study that are ≥20 km in diameter and interpreted as Kuiperian (yellow, identified over 98.4% of Mercury's surface) or Mansurian (red, identified between 40°N and 40°S latitude) in age.

morphologically fresh craters, comparable to Mansur, was formed on Mercury. The end of the Mansurian is loosely defined by the oldest fresh superposing craters with bright ray systems (Figure 1) [*Spudis and Guest*, 1988]. All rayed craters were formed during the Kuiperian period. As is the case for Mansur crater, Kuiper itself is not necessarily the oldest Kuiperian crater using this operational definition.

Having used a similar approach in defining the chronostratigraphic classification for Mercury as was done for the Moon, *Spudis and Guest* [1988] suggested that Mercury's systems are comparable to, but not strictly correlated with, the lunar chronostratigraphic sequence, which is divided into (oldest to youngest) the pre-Nectarian, Nectarian, Imbrian, Eratosthenian, and Copernican [*Shoemaker and Hackman*, 1962; *Stuart-Alexander and Wilhelms*, 1975; *Wilhelms*, 1987]. While assumed to be broadly similar, the duration and onset of corresponding periods in the stratigraphic sequences on Mercury and the Moon were not known to be necessarily the same three decades ago by *Spudis and Guest* [1988] and now are known to be very different (see discussion below). Absolute time constraints have been assigned to the lunar time units by radiometric age dating of samples collected during the Apollo and Luna missions combined with crater counting analyses [e.g., *Vaniman et al.*, 1991; *Stöffler and Ryder*, 2001]. However, radiometric age dating is not currently

possible for Mercury as no samples are available. The most reliable absolute age estimates for the surfaces of Mercury are thus based on extrapolation and correlation of the lunar cratering record to that of Mercury. Similar approaches utilizing crater size-frequency density have been used to estimate model ages for the Martian and Vestan stratigraphic systems [*Tanaka et al*., 2014; *Williams et al*., 2014]. However Mercury has not previously had absolute and relative ages systematically estimated for its complete chronostratigraphic sequence based on crater statistics, particularly for the two most recent periods, the Kuiperian and Mansurian. With the successful imaging of the full surface of Mercury at a range of resolutions and illumination and viewing angles by the MErcury Surface, Space ENviroment, GEochemistry, and Ranging (MESSENGER) spacecraft [*Solomon et al*., 2001], it is now an opportune time to reassess the time scale associated with Mercury's chronostratigraphic systems.

The recent crater model production function (MPF) and inner solar system chronology of *Marchi et al*. [2009] incorporate current knowledge and understanding of impact populations. Using this MPF, *Marchi et al*. [2013] found the oldest pre-Tolstojan surfaces of Mercury to be about 4.0–4.1 Ga and that widespread smooth volcanic plains were emplaced by ~3.6–3.8 Ga during the Calorian. Here we focus on age constraints for Mercury's Mansurian and Kuiperian periods. We use orbital data obtained by the MESSENGER mission [*Solomon et al*., 2001] to catalog impact craters interpreted to be Mansurian and Kuiperian in age. The densities of these crater populations are then used to estimate age boundaries for Mercury's Mansurian and Kuiperian periods.

2. Methods and Data

Morphologically fresh Mansurian- and Kuiperian-aged craters are identified by their crisp and sharp morphologies, well-preserved rims, few or no superposed craters, continuous ejecta with radial lineaments, and well-defined secondary craters [*Arthur et al*., 1963; *Leake*, 1982; *Spudis and Guest*, 1988; *Banks et al*., 2015] (Figure 1). Mercury's youngest craters commonly have bright ray systems (Figure 1a), a diagnostic feature of craters that formed in the Kuiperian. Mansurian craters retain fresh morphologies as described above, but their associated ray systems no longer display a reflectance contrast with the local surrounding surface at visible wavelengths [*Spudis and Guest*, 1988] (Figure 1b). Craters with evidence of more advanced degradation (i.e., subdued rims, substantial infilling of the crater floor, and abundant superposing craters) are interpreted to be Calorian or older in age [*Spudis and Guest*, 1988; *Banks et al*., 2015] and are not included in this analysis. Careful consideration is taken when evaluating the degradation state of craters in close proximity to younger impacts that produced superposing secondary craters and/or ejecta material that could make the crater under evaluation appear more degraded than others of comparable age.

We use high-resolution and multiband images (pixel scales as small as 10 m) and monochrome and color global mosaics (average pixel scales of 250 m) with a diverse range of viewing geometries [*Chabot et al*., 2016], acquired from orbit by the Mercury Dual Imaging System (MDIS) [*Hawkins et al*., 2007] on board MESSENGER, to catalog impact craters interpreted to have formed during the Mansurian and Kuiperian periods (Figure 1c and Tables S1 and S2). For this study, we revise an older catalog of Kuiperian craters first presented by *Xiao et al*. [2012] using more recently available MESSENGER data. The Kuiperian catalog includes rayed craters identified over 98.4% of Mercury's surface (Figures 1c and 2 and Table S1). We use several different data sets to identify and confirm rayed craters including a monochrome low-incidence angle base map (166 m/pixel, optimized to view surface reflectance variations), color mosaics including a global eight-color map (665 m/pixel, 430, 480, 560, 630, 750, 830, 900, and 1000 nm), a high-resolution three-color map (332 m/pixel scales of 50), a north polar five-color map (minimizes phase angles, 332 m/pixel, 430, 560, 750, 830, and 1000 nm), and RGB (1000, 750, and 430 nm) and RGB (750, 430, 410 nm) MDIS images [*Chabot et al*., 2016]. The population of craters interpreted to have formed since the onset of the Mansurian includes all Mansurian- and Kuiperian-aged craters identified on Mercury's surface between 40° north and 40° south latitude. For our Mansurian population, we revise the data set of Mansurian craters (fresh craters without ray systems) first presented by *Braden and Robinson* [2013] and combine it with the rayed craters in our Kuiperian catalog located within this latitudinal range (Figures 1c and 2 and Table S2). Each Mansurian crater is identified and confirmed using available MESSENGER data, including a morphology base map (166 m/pixel, moderate incidence angles near 68°), and east and west illumination images and maps (high incidence angles near 80°) to accentuate crater

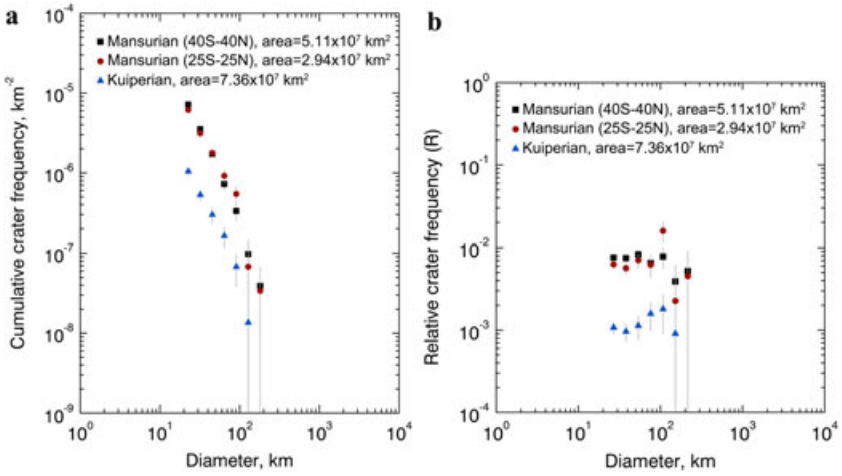

Figure 2. Mansurian (black squares) and Kuiperian (blue triangles) craters used in this study shown in (a) cumulative and (b) relative plots. An independent catalog of Mansurian craters located between 25°N and 25°S latitude [from *Strom et al*., 2015] (red circles) is included for comparison. Plots were generated following standard root 2 binning [*Crater Analysis Techniques Working Group*, 1979].

morphology [*Chabot et al*., 2016]. Craters are identified down to at least 7 km diameter to assure that the catalogs are complete at larger diameters (i.e., 20 km in diameter and larger).

We use the production and chronology functions of *Marchi et al*. [2009] and the densities of fresh craters in our data sets to estimate new age limits for the boundaries of the Kuiperian and Mansurian periods. The *Marchi et al*. [2009] MPF is derived from an input impactor size-frequency distribution (SFD) using crater scaling laws and utilizes our most current knowledge and understanding of the impactor populations [i.e., *Bottke et al*. 2002, 2005]. For our purposes, we use the impactor SFD of Near-Earth Objects (NEOs). The *Marchi et al*. [2009] MPF also incorporates the influence of different surface materials such as density and strength. Hard rock (HR) scaling for strengths of $Y_0 = 2 \times 10^7$ Pa (nominal hard rock [*Asphaug et al*., [1996]), 2×10^6 Pa, and 2×10^5 Pa are applied to investigate a range of model ages [*Holsapple and Housen*, 2007] (also see Text S1). Figure S1 shows impactor diameter versus crater diameter for the different scaling law scenarios applied in this study. Other values include a target density of 3.4 g/cm^3 and an impactor density of 2.6 g/cm^3 (average NEO density). Since the craters we use in calculating the model ages are ≥20 km in diameter (see discussion below), their formation is uniquely within the gravity regime with minor effects from target properties. Therefore, a uniform target is assumed with no layering and no variation of mechanical properties with depth. The *Marchi et al*. [2009] MPF uses the most probable impact angle of 45° and a full distribution of possible impact speeds on Mercury [see *Marchi et al*., 2009]. Crater SFDs are fit to the production function derived from NEOs. While we focus the results reported here on model age estimates obtained with the *Marchi et al*. [2009] MPF, we also include estimated model ages using the production function (PF) of *Le Feuvre and Wieczorek* [2011] (see below and discussion in Text S2).

3. Completeness of the Crater Populations, Size-Dependent Crater Degradation, and Secondaries

We assume that our population of fresh craters (all Mansurian and Kuiperian craters) is a complete catalog of craters that formed since the onset of the Mansurian. Many lunar studies have shown that the topography of smaller lunar craters degrades faster than does the topography of larger craters [e.g., *Pohn and Offield*, 1970; *Soderblom and Lebofsky*, 1972; *Fassett and Thomson*, 2014; *Trang et al*., 2015] and that craters less than ~10 km in diameter lose their optical rays faster than those of larger craters [*Grier et al*., 1998, 2001; *Morota and Furumoto*, 2003; *Braden and Robinson*, 2013].

However, the critical issue for this study is the crater diameter at which morphological degradation and/or fading of crater rays prevents smaller-scale craters from being correctly identified as Mansurian or Kuiperian in age. Based on the work of *Trask* [1971] and *Moore et al*. [1980], lunar craters >10 km are

expected to maintain their topography, only slightly subdued, from the beginning of the Eratosthenian to the present. This is also consistent with analysis of crater degradation rates based on recent measurements of lunar crater topography by *Fassett and Thomson* [2014]. Additionally, while compositional variations can contribute to the formation of crater rays on the Moon [*Hawke et al*., 2004], Mercury's crater rays primarily result from optically immature materials being deposited on the surface by impact processes [*Neish et al*., 2013]. Two major mechanisms lead to the fading of optical crater rays: 1) high-energy solar ultraviolet irradiation and cosmic ray bombardment and 2) impact gardening of the regolith by meteorite bombardment which mixes the ray material with the regolith [*Shoemaker and Hackman*, 1962; *McKay et al*., 1991]. Previous studies by *Morota and Furumoto* [2003] and *Grier et al*. [2001] found that the density of lunar rayed craters $<$10 km in diameter was below the general trend of larger lunar rayed craters and postmare craters. This deficiency of craters $<$10 km in diameter was attributed to a possible size dependency on the longevity of crater rays in which rays of smaller craters darken more rapidly, causing the rays associated with craters $<$10 km to be obliterated at a faster rate than rays associated with larger craters [*Grier et al*., 1998, 2001]. A similar dip in crater density at ~10 km diameter was noticed in the Kuiperian data of this study (Figure S2). However, such size-dependent effects are expected to be minimal once above a certain crater size, which we suggest here is $\geq$20 km diameter. As is the case in previous lunar studies [*Morota and Furumoto*, 2003; *Grier et al*., 1998, 2001], there is no deviation in the density of rayed craters $\geq$~20 km in diameter in our Kuiperian population (see Figures 2 and S2).

To avoid the possibility that some smaller Kuiperian or Mansurian craters may not be included in our populations due to faster morphological degradation or darkening of rays, we limit our model age fits for both the Mansurian and Kuiperian populations to craters $\geq$20 km. To further test the completeness of the data at diameters $\geq$20 km, additional model age fits were completed while adjusting the minimum cutoff crater diameter (i.e., to craters $>$30 km in diameter). These fits were found to be essentially the same as for craters $\geq$20 km in diameter and yield the same estimated model ages (within error bars). Additionally, the consistency in the SFD slope for the Mansurian and Kuiperian populations argues that for craters $\geq$20 km in diameter, size-dependent preservation effects are unlikely to be very significant. If important, such effects would be expected to cause slope deviations in the SFDs, particularly at small sizes. At much larger sizes, it is plausible that a few large craters (i.e., $>$100 km in diameter) that are older than the Mansurian could be mischaracterized as Mansurian craters. However, this is unlikely to affect the estimated model ages reported here outside of the given error bars; craters in this size range ($>$100 km in diameter) have minimal influence on age estimates because these determinations are mostly sensitive to the more numerous smaller craters.

Additionally, statistically significant undetected distal secondaries $\geq$20 km in diameter are not expected to be included in our catalogs as few Mansurian and Kuiperian primaries are sufficiently large to produce secondaries of this scale (i.e., no rayed impact craters/basins $\gg$140 km are confirmed on Mercury). Widespread smooth volcanic plains are estimated to have been emplaced in the Calorian by ~3.6 Ga [*Marchi et al*., 2013; *Denevi et al*., 2013; *Byrne et al*., 2016]. All Kuiperian and Mansurian craters are interpreted to have formed after widespread plains volcanism had ended [*Spudis and Guest*, 1988; *Byrne et al*., 2016], and thus, crater densities from these populations should not have been significantly altered by volcanic resurfacing processes. We also consider the possibility of a potential imaging bias regarding the population of rayed craters, particularly at high latitudes and near the poles, due to Mercury's near-zero obliquity and MESSENGER's elliptical, polar orbit. To investigate this potential effect, rayed crater density is compared for different latitude bands and found to be consistent for $D \geq 7$ km with no detectable latitudinal variations (Figure S2). Providing further support for completeness, an independent catalog of Mansurian and Kuiperian craters located between 25° north and 25° south latitude from *Strom et al*. [2015] is utilized for comparison of results and found to yield similar crater densities and size-frequency distributions (Figure 2). In addition, we cross correlate our Mansurian and Kuiperian craters larger than ~40 km diameter with the data set of *Kinczyk et al*. [2016] to assure that our interpretations of the degradation state of these craters are consistent with that of multiple investigators and studies.

4. Results

4.1. Mansurian

To enable quantitative comparison of crater populations across different studies and assessment of relative ages of different geologic units, we investigate the relative crater frequency by calculating the cumulative

Table 1. Relative Crater Frequencies (Cumulative Number of Craters Equal to or Larger Than a Given Diameter D, $N(D)$, Normalized to an Area of 10^6 km^2)[a]

Time Interval	Crater Densities	
	$N(20)$	$N(30)$
Kuiperian	1.3 ± 0.1	0.6 ± 0.1
Mansurian	8.9 ± 0.4	4.1 ± 0.3
Calorian		
Caloris Basin Rim	41 ± 9[b]	NA
Caloris Basin Interior	29 ± 4[b]	NA
Tolstojan		
Tolstoj Basin: Goya Formation	93 ± 15[b]	NA

[a]Error range is ±1 standard deviation or the square root of the number of craters normalized to an area of 10^6 km^2 [e.g., *Crater Analysis Techniques Working Group*, 1979; *Neukum*, 1983; *Fassett et al*., 2009; *Ostrach et al*., 2015].

[b]*Ernst et al*., [2017]. Recent spatial density results are included for the Calorian and Tolstojan for reference and comparison. Error range calculated using the same method as used in this study (±1 standard deviation).

number of craters equal to or larger than a given diameter D, $N(D)$, normalized to an area of 10^6 km^2 [e.g., *Crater Analysis Techniques Working Group*, 1979; *Neukum*, 1983; *Ostrach et al*., 2015]. Using craters in our catalogs located equatorward of 40° latitude, we find that the number of craters formed since the onset of the Mansurian $N(20)$ with a diameter $D \geq 20$ km is 8.9 ± 0.4. For craters having $D \geq 30$ km, we find $N(30) = 4.1 \pm 0.3$ (Table 1). Following standard technique, the reported error range is ±1 standard deviation or the square root of the number of craters normalized to an area of 10^6 km^2 [e.g., *Crater Analysis Techniques Working Group*, 1979; *Fassett et al*., 2009]. Table 1 summarizes our spatial density results. For reference and comparison, we include recent spatial density results for the Calorian and Tolstojan [*Ernst et al*., 2017].

Using the same data set, estimated absolute model ages of ~1.7–1.8 Ga are obtained using HR (hard rock) scaling for strengths of 2×10^5–2×10^7 Pa, respectively (Figure 3; craters ≥20 km in diameter). We include $Y_0 = 2 \times 10^7$ and 2×10^5 Pa here to assess a wide range of relevant model ages, although hard rock is unlikely to have such a high and low strength, respectively. For comparison, we use the independent data set of craters from *Strom et al*. [2015] (Mansurian and Kuiperian craters equatorward of 25° latitude, Figure 2) with HR strength of 2×10^6 Pa to obtain a model age of ~1.6 Ga, essentially indistinguishable from the model

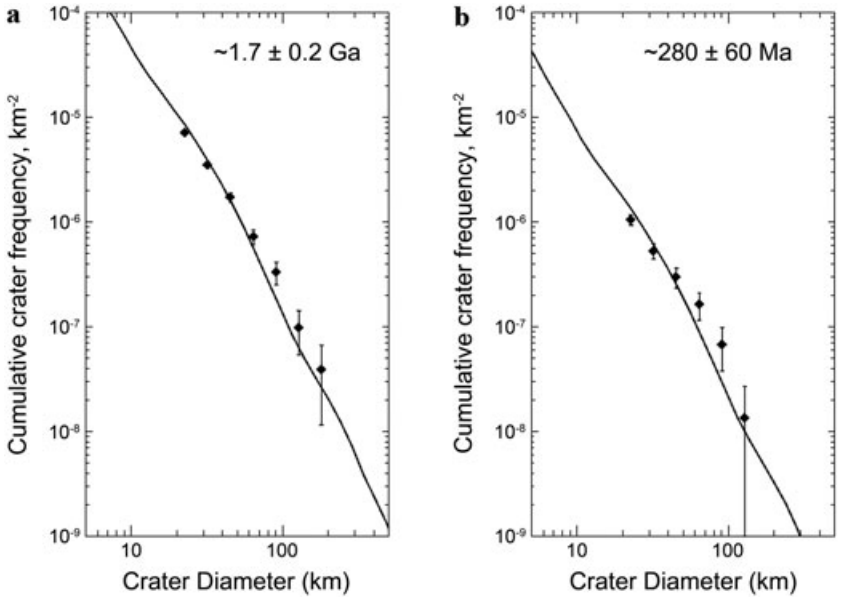

Figure 3. Plots showing estimated model ages for Mercury's populations of craters that formed since the onset of the (a) Mansurian and (b) Kuiperian. Results were derived using the MPF and chronology function of *Marchi et al*. [2009], a NEO-like SFD, and HR scaling for a strength of $Y_0 = 2 \times 10^6$ Pa. Plots were generated following standard root 2 binning [*Crater Analysis Techniques Working Group*, 1979].

Table 2. Summary of Age Estimates for the Kuiperian and Mansurian[a]

	Approximate Age of Onset		
Time Interval	Assumed by *Spudis and Guest* [1988]	From the PF of *Le Feuvre and Wieczorek* [2011]	From the PF of *Marchi et al.* [2009]
Kuiperian	1.0 Ga	130 Ma	280 Ma
Mansurian	3.0–3.5 Ga	850 Ma	1.7 Ga

[a]Ages from *Spudis and Guest* [1988] are included for reference.

ages found for the population used in this study. Altogether, we estimate a model age for the population of craters that have formed since the onset of the Mansurian period of ~1.7 ± 0.2 Ga (Figure 3; formal model errors are derived out of a best fitting routine that minimizes the chi-square difference between the data and the model).

4.2. Kuiperian

For the number of craters formed since the onset of the Kuiperian with diameters $D \geq 20$ km, we find $N(20) = 1.3 \pm 0.1$. For craters with $D \geq 30$ km, we find $N(30) = 0.6 \pm 0.1$ (Table 1). Absolute model ages are estimated for our Kuiperian population using the same range of values as was used for the Mansurian population (craters ≥20 km in diameter). Estimated model ages range from ~280 to 290 Ma for our assumed strengths. Considering our range of relevant results together, we estimate a model age of ~280 ± 60 Ma (Figure 3, formal model errors) for the population of craters formed since the onset of the Kuiperian period.

4.3. Estimated Model Ages From the Production Function of *Le Feuvre and Wieczorek* [2011]

Le Feuvre and Wieczorek [2011] also developed a PF for inner solar system bodies (also see discussion in Text S2 regarding the work of *Neukum et al.* [2001]). The *Le Feuvre and Wieczorek* [2011] PF utilizes the same asteroid catalog and a similar calculation procedure to that of *Marchi et al.* [2009] but incorporates a slightly different impactor population (the orbital distribution of near-Earth objects of *Bottke et al.* [2002], modified for Mars), different parameters for target materials in applying crater scaling laws, a different diameter ratio of transient to final crater size, and a different transition diameter for simple to complex craters [see *Le Feuvre and Wieczorek*, 2011]. Utilizing the work of *Le Feuvre and Wieczorek* [2011], and again limiting our model age fits to craters ≥20 km in diameter, we estimate a model age for the onset of the Mansurian and Kuiperian of ~850 Ma and ~130 Ma, respectively (Figure S3). For these model age estimates, we use the nonporous scaling regime because the diameter range of the crater populations used in this study (≥20 km in diameter) is greater than that used with the porous scaling regime as defined by *Le Feuvre and Wieczorek* [2011].

Table 2 summarizes estimated model ages. As discussed above, we focus on results obtained with the *Marchi et al.* [2009] MPF and investigate a range of surface material strengths and other values to assess the possible range of relevant model ages. The causes of the differences in estimated model ages derived from the work of *Marchi et al.* [2009] and *Le Feuvre and Wieczorek* [2011] are unclear. Comparisons between the two approaches indeed show differences in the production and chronology functions that result in differences in age determinations [see *Le Feuvre and Wieczorek*, 2011, Figures 2 and 8], especially for the size range of interest for this study. As is noted in *Le Feuvre and Wieczorek* [2011], it is difficult to quantify the effect of the various differences in the two approaches on the final crater SFD (and thus the derived surface age). *Le Feuvre and Wieczorek* [2011] point to the differing crater scaling laws as perhaps significant.

Most importantly, results using the work of both *Marchi et al.* [2009] and *Le Feuvre and Wieczorek* [2011] point consistently to significantly more recent onsets and substantially shorter durations of the Mansurian (≥~40% shorter) and Kuiperian (≥~70% shorter) than previously assumed (Table 2). In other words, while there are differences between the implied absolute ages, results using the work of both studies [*Marchi et al.*, 2009; *Le Feuvre and Wieczorek*, 2011] are in qualitative agreement with respect to the shortening of the Mansurian and Kuiperian.

5. Discussion

Craters formed during the Mansurian (~1.7–0.28 Ga) and Kuiperian (<~280 Ma) are morphologically classified the same as craters formed during the lunar Eratosthenian (~3.2–0.8 Ga) [*Wilhelms*, 1987; *Neukum and Ivanov*,

1994, *Stöffler and Ryder*, 2001] and Copernican (<~800 Ma) [*Stöffler and Ryder*, 2001], respectively. Shorter time scales for the Mansurian and Kuiperian compared to the corresponding lunar periods are consistent with results from previous studies that predict higher crater degradation rates for Mercury compared to the Moon [i.e., *Fassett and Crowley*, 2016]. For example, Mercury has a greater total impact flux and higher mean impact velocities [*Gault et al*., 1975; *Cintala*, 1992; *Le Feuvre and Wieczorek*, 2011; *Domingue et al*., 2014; *Kreslavsky et al*., 2014] than the Moon, which increases the amount of erosion from subsequent cratering [*Gault et al*., 1975; *Spudis and Guest*, 1988, *Cintala*, 1992; *Le Feuvre and Wieczorek*, 2011; *Domingue et al*., 2014]. Mercury's higher surface gravitational acceleration also causes material ejected from a primary crater to impact the surface at a greater velocity [*Scott*, 1977; *Xiao et al*., 2014] and thus with greater erosive power [*Spudis and Guest*, 1988]. In addition, secondary craters are much larger and more numerous on Mercury compared with the Moon for primary craters of equal sizes [*Gault et al*., 1975; *Strom et al*., 2011; *Xiao*, 2016]. A greater total impact flux and higher mean impact velocity is consistent with a regolith thickness on Mercury that is 3 times greater than that of the Moon on average [*Kreslavsky et al*., 2014]. Craters of similar sizes and states of degradation would thus be expected to be younger on Mercury than on the Moon. Recent studies have also found optical maturation rates to be up to 4 times faster on Mercury than on the Moon due to the combined effect of the larger impact flux, faster degradation rates, and greater intensity of solar wind bombardment [*Braden and Robinson*, 2013; *Neish et al*. 2013; *Kreslavsky et al*., 2014], consistent with a younger age for the Kuiperian crater population.

We do not know that the currently observed best production function for NEOs has been constant over earlier epochs. Thus, we use a slightly different test SFD to explore the degree to which alternative SFDs, modestly different from our baseline model, might affect our conclusions (see Figures 3 and S4). Using the same values detailed above (i.e., $Y_0 = 2 \times 10^6$ Pa, target and impactor densities of 3.4 g/cm^3 and 2.6 g/cm^3, respectively) and applying our test SFD, we obtain similar estimated model ages (within error bars) of ~1.4 ± 0.2 Ga and ~220 ± 60 Ma for the Mansurian and Kuiperian, respectively (Figure S4). The fit for our test SFD exhibits a shallower slope at large crater sizes improving the quality of the fit in this size range (Figures 3 and S4). It is possible that averaged over the last 2 Gyr, the true NEO impact SFD at Mercury may somewhat deviate from the debiased overall NEO SFD. A detailed investigation of this, however, is left for future work. The quality of these fits could also be affected by observational or preservation biases such as the size dependency of crater and ray degradation as discussed above in section 3.

Knowledge of the absolute time scales associated with the Kuiperian and Mansurian periods is critical for understanding the timing of all major stratigraphic periods on Mercury and provides significant constraints for the interpretation, modeling, and analysis of Mercury's geologic, thermal, and tectonic evolution. Since, by definition, the Calorian ends when the Mansurian begins, the results presented here suggest that the Calorian period may have been more than 2 times longer than previously assumed, extending in duration well past the cessation of volcanism associated with Mercury's youngest widespread smooth plains, ~3.6 Ga [*Spudis and Guest*, 1988; *Marchi et al*., 2013; *Denevi et al*., 2013; *Byrne et al*., 2016]. Younger onset ages also are relevant to the timing of processes established as Mansurian and Kuiperian in age, such as hollow formation [e.g., *Blewett et al*., 2011, 2013; *Vaughan et al*., 2012], tectonism [e.g., *Xiao et al*., 2012; *Banks et al*., 2014, 2015; *Watters et al*., 2016], and pyroclastic volcanism [e.g., *Kerber et al*., 2009, 2011; *Gillis-Davis et al*., 2009; *Goudge et al*., 2013; *Denevi et al*., 2013; *Rothery et al*., 2014], and the potential for these processes to have been active geologically recently and, for some, possibly ongoing today.

For example, crosscutting relationships between lobate scarps and craters in different stages of degradation [*Banks et al*., 2015] show that thrust faulting on Mercury, attributed primarily to long-term shortening of the lithosphere in response to cooling and contraction of the planetary interior [e.g., *Strom et al*., 1975; *Watters et al*., 1998; *Strom and Sprague*, 2003; *Solomon et al*., 2008; *Watters and Nimmo*, 2010], initiated at least within the Calorian and continued through the Mansurian [*Banks et al*., 2015]. Evidence of recent contraction on some large-scale tectonic structures and observations of small-scale contractional structures point to thrust faulting continuing into the Kuiperian [*Xiao et al*., 2012; *Banks et al*., 2014, 2015; *Watters et al*., 2016]. These findings, in concert with the revised time scales presented here, support interior thermal evolution models that predict the onset of global contraction of Mercury near the end of the LHB and continuing to within the last ~280 Ma and likely to the present [e.g., *Hauck et al*., 2004; *Michel et al*., 2013; *Tosi et al*., 2013].

Based on crosscutting relationships with fresh craters, MESSENGER orbital observations also reveal evidence for Mansurian- and Kuiperian-aged pyroclastic eruptions [*Kerber et al*., 2009, 2011; *Gillis-Davis et al*., 2009; *Goudge et al*., 2013; *Denevi et al*., 2013; *Rothery et al*., 2014]. These findings indicate not only that volcanism has continued much more recently than the time of emplacement of most smooth plains deposits [*Xiao et al*., 2012; *Goudge et al*., 2013; *Thomas et al*., 2014] but also that it has continued through to much more geologically recent times than previously understood. As global contraction imposes a stress state on Mercury's lithosphere that inhibits the ascent of magma to the surface [*Solomon*, 1978], lithosphere buckling had potentially not yet sealed all the conduits for the pressurized partial melting of the mantle to upwell as of the onset of the Kuiperian. Mercury's young pyroclastic volcanic features, however, are primarily associated with impact craters in which preexisting stresses would have been removed facilitating the ascent of mantle-derived magma. Some of these volcanic features are also associated with thrust faults, in which the faults could have served as conduits for the vertical ascent of volatile-rich magmas [*Kerber et al*., 2009; *Klimczak et al*., 2013]. Interestingly, no substantial variations in the ultraviolet to near-infrared reflectance spectra are detected for different-aged pyroclastic deposits on Mercury, suggesting that the mantle source has not substantially changed through time [*Kerber et al*., 2009, 2011; *Goudge et al*., 2013].

6. Summary and Conclusions

We use populations of fresh craters on Mercury to constrain age boundaries for the Mansurian and Kuiperian periods. Results indicate that both the Mansurian and Kuiperian have shorter time scales and began much more recently than the lunar Eratosthenian and Copernican, respectively. Although different PFs [*Marchi et al*., 2009; *Le Feuvre and Wieczorek*, 2011] yield differing estimated model ages (Table 2), they consistently indicate ages for the onset of the Mansurian and Kuiperian periods that are significantly more recent than the previously assumed onset ages of ~3.5–3.0 Ga and ~1.0 Ga, respectively [*Spudis and Guest*, 1988]. Results presented here indicate time spans for the Mansurian and Kuiperian that are ≥~40% and ≥~70% shorter in duration, respectively, than previously assumed [*Spudis and Guest*, 1988]. A more recent onset of the Mansurian also points to a significantly longer time span for the Calorian period (previously assumed to be ~400–900 Myr in duration), which may have extended roughly another 2 billion years after the cessation of volcanism associated with Mercury's youngest widespread smooth plains, ~3.6 Ga [*Marchi et al*., 2013; *Denevi et al*., 2013; *Byrne et al*., 2016]. Based on the work of *Marchi et al*. [2009], we estimate that the Mansurian period began as recently as ~1.7 ± 0.2 Ga and the Kuiperian as recently as ~280 ± 60 Ma (Figure 3 and Table 2).

Acknowledgments
Data are available from the NASA Planetary Data System (https://pds.nasa.gov/). Results from the crater analyses are included in Tables S1 and S2 in the supporting information. This work was supported by NASA grant NNX07AR60G. S. Marchi acknowledges support from NASA SSERVI. The MESSENGER project was supported by the NASA Discovery Program under contracts NASW-00002 to the Carnegie Institution of Washington and NAS5-97271 to The Johns Hopkins University Applied Physics Laboratory. We thank L.R. Ostrach, G. Michael, D. Baratoux, and an anonymous reviewer for their helpful input and reviews of this manuscript. We also thank the entire MESSENGER team, R.G. Strom, and M. Kinczyk for their helpful input and support for this investigation.

References

Arthur, D. W. G., A. P. Agneray, R. A. Horvath, C. A. Wood, and C. R. Chapman (1963), The system of lunar craters, quadrant I, *Commun. Lunar Planet. Lab*, *2*, 71–78.

Asphaug, E., J. M. Moore, D. Morrison, W. Benz, M. C. Nolan, and R. J. Sullivan (1996), Mechanical and geological effects of impact cratering on Ida, *Icarus*, *120*, 158, doi:10.1006/icar.1996.0043.

Banks, M. E., C. Klimczak, Z. Xiao, T. R. Watters, R. G. Strom, S. E. Braden, C. R. Chapman, S. C. Solomon, and P. K. Byrne (2014), Duration of activity on lobate-scarp thrust faults on Mercury, *Lunar Planet. Sci.*, *45*, Abstract 2722.

Banks, M. E., Z. Xiao, T. R. Watters, R. G. Strom, S. E. Braden, C. R. Chapman, S. C. Solomon, C. Klimczak, and P. K. Byrne (2015), Duration of activity on lobate-scarp thrust faults on Mercury, *120*, 1751–1762, doi:10.1002/2015JE004828.

Braden, S. E., and M. S. Robinson (2013), Relative rates of optical maturation of regolith on Mercury and the Moon, *J. Geophys. Res. Planets*, *118*, 1903–1914, doi:10.1002/jgre.20143.

Blewett, D. T., et al. (2011), Hollows on Mercury: MESSENGER evidence for geologically recent volatile-related activity, *Science*, *333*, 1856–1859, doi:10.1126/science.1211681.

Blewett, D. T., et al. (2013), Mercury's hollows: Constraints on formation and composition from analysis of geological setting and spectral reflectance, *J. Geophys. Res. Planets*, *118*, 1013–1032, doi:10.1029/2012JE004174.

Bottke, W. F., A. Morbidelli, R. Jedicke, J.-M. Petit, H. F. Levison, P. Michel, and T. S. Metcalfe (2002), Debiased orbital and absolute magnitude distribution of the near-Earth objects, *Icarus*, *156*, 399–433, doi:10.1006/icar.2001.6788.

Bottke, W. F., D. D. Durda, D. Nesvorn'y, R. Jedicke, A. Morbidelli, D. Vokrouhlick'y, and H. F. Levison (2005), Linking the collisional history of the main asteroid belt to its dynamical excitation and depletion, *Icarus*, *1*(179), 63–94, doi:10.1016/j.icarus.2005.05.017.

Byrne, P. K., L. R. Ostrach, C. I. Fassett, C. R. Chapman, B. W. Denevi, A. J. Evans, C. Klimczak, M. E. Banks, J. W. Head, and S. C. Solomon (2016), Widespread effusive volcanism on Mercury likely ended by about 3.5 Ga, *Geophys. Res. Lett.*, *43*, 7408–7416, doi:10.1002/2016GL069412.

Chabot, N. L., B. W. Denevi, S. L. Murchie, C. D. Hash, C. M. Ernst, D. T. Blewett, H. Nair, N. R. Laslo and S. C. Solomon (2016), Mapping Merucry: Global imaging strategy and products from the MESSENGER mission, *Lunar Planet. Sci.*, *47*, Abstract 1256.

Cintala, M. J. (1992), Impact-induced thermal effects in the lunar and Mercurian regoliths, *J. Geophys. Res.*, *97*, 947–973, doi:10.1029/917JE0220.

Crater Analysis Techniques Working Group, R. Arvidson, et al. (1979), Standard techniques for presentation and analysis of crater size-frequency data, *Icarus*, *37*, 467–474, doi:10.1016/0019-1035(79)90009-5.

Denevi, B. W., and M. S. Robinson (2008), Mercury's albedo from Mariner 10: Implications for the presence of ferrous iron, *Icarus*, *197*, 239–246, doi:10.1016/j.icarus.2008.04.021.
Denevi, B. W., et al. (2013), The distribution and origin of smooth plains on Mercury, *J. Geophys. Res. Planets*, *118*, 891–907, doi:10.1002/jgre.20075.
Domingue, D. L., et al. (2014), Mercury's weather-beaten surface: Understanding Mercury in the context of lunar and asteroidal space weathering studies, *Space Sci. Rev.*, *181*, 121–214, doi:10.1007/s11214-014-0039-5.
Ernst, C. M., Denevi, B. W., and Ostrach, L. R. (2017) Updated absolute age estimates for the Tolstoj and Caloris basins, Mercury, Lunar Planet. Sci, 48, Abstract 2934.
Fassett, C. I., and B. J. Thomson (2014), Crater degradation on the lunar maria: Topographic diffusion and the rate of erosion on the Moon, *J. Geophys. Res. Planets*, *119*, 2255–2271, doi:10.1002/2014JE004698.
Fassett, C. I. and M. C. Crowley (2016) High-resolution stereo digital terrain models of Mercury: Degradation and morphometry, *Lunar Planet. Sci*, 47, Abstract 1046.
Fassett, C. I., J. W. Head, D. T. Blewett, C. R. Chapman, J. L. Dickson, S. L. Murchie, S. C. Solomon, and T. R. Watters (2009), Caloris impact basin: Exterior geomorphology, stratigraphy, morphometry, radial sculpture, and smooth plains deposits, *Earth Planet. Sci. Lett.*, *285*, 297–308, doi:10.1016/j.epsl.2009.05.022.
Gault, D. E., J. E. Guest, J. B. Murray, D. Dzurisin, and M. C. Malin (1975), Some comparisons of impact craters on Mercury and the Moon, *J. Geophys. Res.*, *80*, 2444–2460, doi:10.1029/JB080i017p02444.
Gillis-Davis, J. J., D. T. Blewett, R. W. Gaskell, B. W. Denevi, M. S. Robinson, R. G. Strom, S. C. Solomon, and A. L. Sprague (2009), Pit-floor craters on Mercury: Evidence of near-surface igneous activity, *Earth Planet. Sci. Lett.*, *285*, 243–250.
Goudge, T. A., et al. (2013), Global inventory and characterization of pyroclastic deposits on Mercury: New insights into pyroclastic activity from MESSENGER orbital data, *J. Geophys. Res. Planets*, *119*, 635–658, doi:10.1002/2013JE004480.
Grier, J. A., A. S. McEwen, C. Aragon, R. G. Strom, and J. Ingram (1998), A preliminary look at bright lunar craters using the Clementine global mosaic, *Lunar Planet. Sci.*, *29*, Abstract 1905.
Grier, J. A., A. S. McEwen, P. G. Lucey, M. Milazzo, and R. G. Strom (2001), Optical maturity of ejecta from large rayed lunar craters, *J. Geophys. Res.*, *106*, 32,847–32,862, doi:10.1029/1999JE001160.
Hauck, S. A., II, A. J. Dombard, R. J. Phillips, and S. C. Solomon (2004), Internal and tectonic evolution of Mercury, *Earth Planet. Sci. Lett.*, *222*, 713–728, doi:10.1016/j.epsl.2004.03.037.
Hawke, B., D. Ray, T. Blewett, P. G. Lucey, G. A. Smith, J. F. Bell III, B. A. Campbell, and M. S. Robinson (2004), The origin of lunar crater rays, *Science*, *170*, 1–16, doi:10.1016/j.icarus.2004.02.013.
Hawkins, S. E., III, et al. (2007), The Mercury Dual Imaging System on the MESSENGER spacecraft, *Space Sci. Rev.*, *131*, 247–338.
Holsapple, K. A., and K. R. Housen (2007), A crater and its ejecta: An interpretation of deep impact, *Icarus*, *191*(2), 586–597, doi:10.1016/j.icarus.2006.08.035.
Kinczyk, M. J., L. M. Prockter, C. R. Chapman, and H. C. M. Susorney (2016), A morphological evaluation of crater degradation on Mercury: Revisiting crater classification with MESSENGER data, *Lunar Planet. Sci.*, *47*, Abstract 1573.
Kerber, L., J. W. Head, S. C. Solomon, S. L. Murchie, D. T. Blewett, and L. Wilson (2009), Explosive volcanic eruptions on Mercury: Eruption conditions, magma volatile content, and implications for interior volatile abundances, *Earth Planet. Sci. Lett.*, *285*, 263–271, doi:10.1016/j.epsl.2009.04.037.
Kerber, L., J. W. Head, D. T. Blewett, S. C. Solomon, L. Wilson, S. L. Murchie, M. S. Robinson, B. W. Denevi, and D. L. Domingue (2011), The global distribution of pyroclastic deposits on Mercury: The view from MESSENGER flybys 1–3, *Planet. Space Sci.*, *59*, 1895–1909, doi:10.1016/j.pss.2011.03.020.
Klimczak, C., P. K. Byrne, and S. C. Solomon, F. Nimmo, T. R. Watters, B. W. Denevi, C. M. Ernst, and M. E. Banks (2013), The role of thrust faults as conduits for volatiles on Mercury, *Lunar Planet. Sci.*, *44*, Abstract 1390.
Kreslavsky, M. A., J. W. Head, G. A. Neumann, M. T. Zuber, and D. E. Smith (2014), Kilometer scale topographic roughness of Mercury: Correlation with geologic features and units, *Geophys. Res. Lett.*, *41*, 8245–8251, doi:10.1002/2014GL062162.
Leake, M. A. (1982), The intercrater plains of Mercury and the Moon: Their nature, origin, and role in terrestrial planet evolution, in *Advances in Planetary Geology*, Technical Memorandum TM-84894, pp. 3–535, NASA, Washington, D. C.
Le Feuvre, M., and M. A. Wieczorek (2011), Nonuniform cratering of the Moon and a revised crater chronology of the inner solar system, *Icarus*, *214*, 1–20, doi:10.1016/j.icarus.2011.03.010.
Marchi, S., S. Mottola, G. Cremonese, M. Massironi, and E. Martellato (2009), A new chronology for the Moon and Mercury, *Astrophys. J.*, *137*, 4936–4948.
Marchi, S., C. R. Chapman, C. I. Fassett, J. W. Head, W. F. Bottke, and R. G. Strom (2013), Global resurfacing of Mercury 4.0–4.1 billion years ago by heavy bombardment and volcanism, *Nature*, *499*, 59–61, doi:10.1038/nature12280.
McKay, D. S., G. Heiken, A. Basu, G. Blanford, S. Simon, R. Reedy, B. French, and J. Papike (1991), The lunar regolith, in *The Lunar Source Book: A User's Guide to the Moon*, edited by G. Heiken, D. T. Vaniman, and B. French, pp. 285–356, Cambridge Univ. Press, Cambridge.
Michel, N. C., S. A. Hauck II, S. C. Solomon, R. J. Phillips, J. H. Roberts, and M. T. Zuber (2013), Thermal evolution of Mercury as constrained by MESSENGER observations, *J. Geophys. Res. Planets*, *118*, 1033–1044, doi:10.1002/jgre.20049.
Moore, H. J., J. M. Boyce, and D. A. Hahn (1980), Small impact craters in the lunar regolith—Their morphologies relative ages and rates of formation, *Moon Planets*, *23*, 231–252.
Morota, T., and M. Furumoto (2003), Asymmetrical distribution of rayed craters on the Moon, *Earth Planet. Sci. Lett.*, *206*, 315–323, doi:10.1016/S0012821X(02)011111.
Neish, C. D., D. T. Blewett, J. K. Harmon, E. I. Coman, J. T. S. Cahill, and C. M. Ernst (2013), A comparison of rayed craters on the Moon and Mercury, *J. Geophys. Res. Planets*, *118*, 2247–2261, doi:10.1002/jgre.20166.
Neukum, G. (1983), Meteoritenbombardement and Datierung planetarer Oberflächen. Habilitation Dissertation for faculty membership, Univ. of Munich, 186 pp.
Neukum, G., and B. A. Ivanov (1994), Crater size distributions and impact probabilities on earth from lunar, terrestrial planet, and asteroid cratering data, in *Hazards Due to Comets and Asteroids*, edited by T. Gehrels, pp. 359–416, Univ. of Arizona Press, Tucson, Ariz.
Neukum, G., J. Oberst, H. Hoffmann, R. Wagner, and B. A. Ivanov (2001), Geologic evolution and cratering history of Mercury, *Planet. Space Sci.*, *49*, 1507–1521.
Ostrach, L. R., M. S. Robinson, J. L. Whitten, C. I. Fassett, R. G. Strom, J. W. Head, and S. C. Solomon (2015), Extent, age, and resurfacing history of the northern smooth plains on Mercury from MESSENGER observations, *Icarus*, *250*, 602–622.
Pohn, H. A., and T. W. Offield (1970), Lunar crater morphology and relative age determination of lunar geologic units—Part 1. Classification, *U.S. Geol. Surv. Prof. Pap.*, *700-C*, C153–C162.

Rothery, D. A., R. J. Thomas, and L. Kerber (2014), Prolonged eruptive history of a compound volcano on Mercury: Volcanic and tectonic implications, *Earth Planet. Sci. Lett.*, *385*, 59–67.
Scott, D. H. (1977), Moon–Mercury: Relative preservation states of secondary craters, *Phys. Earth Planet. Inter.*, *15*, 173–178.
Shoemaker, E. M., and R. J. Hackman (1962), Stratigraphic basis for a lunar time scale, in *The Moon*, edited by Z. Kopal and Z. K. Mikhailov, pp. 277–339, Academic Press, New York.
Soderblom, L. A., and L. A. Lebofsky (1972), Technique for rapid determination of relative ages of lunar areas from orbital photography, *J. Geophys. Res.*, *77*, 279–296, doi:10.1029/JB077i002p00279.
Solomon, S. C. (1978), On volcanism and tectonics on one-plate planets, *Geophys. Res. Lett.*, *5*, 461–464, doi:10.1029/GL005i006p00461.
Solomon, S. C., et al. (2001), The MESSENGER mission to Mercury: Scientific objectives and implementation, *Planet. Space Sci.*, *49*, 1445–1465.
Solomon, S. C., et al. (2008), Return to Mercury: A global perspective on MESSENGER's first Mercury flyby, *Science*, *321*, 59–62, doi:10.1126/science.1159706.
Spudis, P. D., and J. E. Guest (1988), Stratigraphy and geologic history of *Mercury*, in *Mercury*, edited by F. Vilas, C. R. Chapman, and M. S. Matthews, pp. 118–164, Univ. of Arizona Press, Tucson, Ariz.
Stöffler, D., and G. Ryder (2001), Stratigraphy and isotope ages of lunar geologic units: Chronological standard for the inner solar system, *Space Sci. Rev.*, *96*, 9–54.
Strom, R. G., and A. L. Sprague (2003) *Exploring Mercury: The Iron Planet*, p. 216, Springer Praxis Books, Chichester, U. K.
Strom, R. G., N. J. Trask, and J. E. Guest (1975), Tectonism and volcanism on Mercury, *J. Geophys. Res.*, *80*, 2478–2507, doi:10.1029/JB080i017p02478.
Strom, R. G., R. Malhotra, T. Ito, F. Yoshida, and D. A. Kring (2005), The origin of planetary impactors in the inner solar system, *Science*, *309*, 1847–1850, doi:10.1126/science.1113544.
Strom, R. G., M. Banks, C. R. Chapman, C. I. Fassett, J. A. Forde, J. W. Head, W. J. Merline, L. M. Prockter, and S. C. Solomon (2011), Mercury crater statistics from MESSENGER flybys: Implications for stratigraphy and resurfacing history, *Planet. Space Sci.*, *59*, 1960–1967, doi:10.1016/j.pss.2011.03.018.
Strom, R. G., R. Malhotra, Z. Xiao, T. Ito, F. Yoshida, and L. R. Ostrach (2015), The inner solar system cratering record and the evolution of impactor populations, *Res. Astron. Astrophys.*, *15*(3), 407–434, doi:10.1088/1674-4527/15/3/009.
Stuart-Alexander, D. E., and D. E. Wilhelms (1975), The Nectarian system: A new lunar time-stratigraphic unit, *J. Res. U. S. Geol. Surv.*, *3*, 53–58.
Tanaka, K. L., J. A. Skinner, Jr., J. M. Dohm, R. P. Irwin, III, E. J. Kolb, C. M. Fortezzo, T. Platz, G. G. Michael, and T. M. Hare (2014), Geologic map of Mars, *U.S. Geological Survey Scientific Investigations Map 3292*, scale 1:20,000,000, pamphlet 43 p., doi:10.3133/sim3292.
Thomas, R. J., D. A. Rothery, S. J. Conway, and M. Anand (2014), Long-lived explosive volcanism on Mercury, *Geophys. Res. Lett.*, *41*, 6084–6092, doi:10.1002/2014GL061224.
Tosi, N., M. Grott, A.-C. Plesa, and D. Breuer (2013), Thermochemical evolution of Mercury's interior, *J. Geophys. Res. Planets*, *118*, 2474–2487, doi:10.1002/jgre.20168.
Trang, D., J. J. Gillis-Davis, and J. M. Boyce (2015), Absolute model ages from lunar crater morphology, *J. Geophys. Res. Planets*, *120*, 725–738, doi:10.1002/2014JE004639.
Trask, N. J. (1971), Geologic comparison of mare materials in the lunar equatorial belt, including Apollo 11 and Apollo 12 landing sites, *U.S. Geol. Surv. Prof. Pap.*, *750D*, 2645–2662.
Vaniman, D., J. Dietrich, G. J. Taylor, and G. H. Heiken (1991), Exploration, samples, and recent concepts of the Moon, in *The Lunar Sourcebook*, edited by G. H. Heiken, D. T. Vaniman, and B. M. French, pp. 5–26, Cambridge Univ. Press, Cambridge.
Vaughan, W. M., J. Helbert, D. T. Blewett, J. W. Head, S. L. Murchie, K. Gwinner, T. J. McCoy, and S. C. Solomon (2012), Hollow-forming layers in impact craters on Mercury: Massive sulfide or chloride deposits formed by impact melt differentiation?, *Lunar Planet. Sci.*, *43*, Abstract 1187.
Watters, T. R., and F. Nimmo (2010), The tectonics of Mercury, in *Planetary Tectonics*, edited by T. R. Watters and R. A. Schultz, pp. 15–80, Cambridge Univ. Press, New York.
Watters, T. R., M. S. Robinson, and A. C. Cook (1998), Topography of lobate scarps on Mercury: New constraints on the planet's contraction, *Geology*, *26*, 991–994.
Watters, T. R., K. Daud, M. E. Banks, M. M. Selvans, C. R. Chapman, and C. M. Ernst (2016), Recent tectonic activity on Mercury revealed by small thrust fault scarps, *Nat. Geosci.*, doi:10.1038/NGEO2814.
Wilhelms, D. E. (1987) *The Geologic History of the Moon*, *U.S. Geol. Surv. Prof. Pap.*, vol. 1348, 302 pp., United States Government Printing Office, Washington, D. C.
Williams, D. S., R. Jaumann, H. Y. McSween Jr., S. Marchi, N. Schmedemann, C. A. Raymond, and C. T. Russell (2014), The chronostratigraphy of protoplanet Vesta, *Icarus*, *244*, 158–165, doi:10.1016/j.icarus.2014.06.027.
Xiao, Z. (2016), Size-frequency distribution of different secondary crater populations: 1. Equilibrium caused by secondary impacts, *J. Geophys. Res. Planets*, *121*, 2404–2425, doi:10.1002/2016JE005139.
Xiao, Z., et al. (2012), The youngest geologic terrains on Mercury, *Lunar Planet. Sci.*, *43*, Abstract 2143.
Xiao, Z., R. G. Strom, C. R. Chapman, J. W. Head, C. Klimczak, L. R. Ostrach, J. Helbert, and P. D'Incecco (2014), Comparisons of fresh complex impact craters on Mercury and the Moon: Implications for controlling factors in impact excavation processes, *Icarus*, *228*, 260–275, doi:10.1016/j.icarus.2013.10.002.